Crystal Refinement and Magnetic Structure of $KNi_4(PO_4)_3$: A Novel Example of Three Interacting Magnetic Sub-Lattices

María-Luisa López, Cristina Durio, Abdelaali Daidouh, Carlos Pico, and María-Luisa Veiga*[a]

Abstract: $KNi_4(PO_4)_3$ has been synthesised following a method previously reported by some of us and studied on the basis of magnetization and neutron powder diffraction (NPD) data. Magnetization measurements suggest the coexistence of ferromagnetic (FM) and antiferromagnetic (AFM) interactions: magnetization versus magnetic field curves present a remanent magnetization of around 2.15 μ_B at $T=2$ K. The magnetic structure of the $KNi_4(PO_4)_3$ has been determined at low temperature from the NPD data. These measurements show that there are three magnetic sub-lattices of Ni^{2+} ions, which interact through common oxygen or phosphate groups, giving rise to FM and AFM couplings. The resulting interactions are FM in nature. Such a complex behaviour could provide an interesting model to analyse magnetic interactions in more condensed systems, such in mixed metal oxides.

Keywords: magnetic properties · neutron diffraction · nickel ·

Introduction

Solid transition-metal compounds are of considerable interest, because they display a plethora of remarkable electrical and magnetic properties. The most studied systems are the transition-metal oxides, with many of them exhibiting noticeable magnetic properties related with either low dimensionality,[1,2] or frustration effects[3] and spin-ice materials,[4] for example. Thus, the understanding of complex electronic and magnetic properties in materials in which electrons are on the edge of itinerant to localised transition needs a clear knowledge of the fundamental magnetic properties of simpler materials, such as the electronic insulators, which could provide useful models to study those more difficult systems.

In this sense, phosphate oxosalts of transition-metal cations are quite close to oxides, because they show a wide range of connections between metal polyhedra, in general with very opened structures, that give rise to various potential applications. Many of them are related to solid-state devices for lithium batteries as electrodes or electrolytes, with $LiFePO_4$ and $LiFe_3(PO_4)_3$[5,6] being some representative examples. On the other hand, transition-metal cations can define three-dimensional condensed frameworks that exhibit interesting cooperative magnetic interactions.[7–10] In particular, the complex structural chemistry of several orthophosphates of general formula $AM_4(PO_4)_3$ (A = alkali metal, M = divalent metal cation) has been studied for many years,[11–17] and different crystal structures have been described.

Phosphates with the above stoichiometry possess orthorhombic symmetries with quite similar unit cell parameters, which mainly depend on the cation sizes (Table 1). Nevertheless, noticeable differences in metal coordination polyhedra and in their connectivities are encountered; this implies varied physical properties. Unfortunately, even if good crys-

Table 1. Othophosphates of general formula $AM_4(PO_4)_3$.

	Space group	a [Å]	b [Å]	c [Å]	Ref.
$KFe_4(PO_4)_3$ (single crystal)	*Pmnn*	6.273	16.513	9.808	[11]
$NaMg_4(PO_4)_3$ (single crystal)	*Pnma*	9.883	6.345	15.240	[12]
$NaNi_4(PO_4)_3$ (single crystal)	*Amam*	9.892	14.842	6.357	[13]
$KMn_4(PO_4)_3$ (single crystal)	*Pmcn*	6.550	16.028	9.977	[14]
$ANi_4(PO_4)_3$ A = Na, K (polycrystal)	*Pmnn*	6.148	16.210	9.474	[15, 16] (this paper)
$KMn_4(PO_4)_3$ (polycrystal)	*Pmnn*	6.554	16.049	9.977	[15, 16]
$(NH_4)Mn_4(PO_4)_3$ (single crystal)	*Pnnm*	9.885	16.745	6.464	[17]

[a] Prof. M.-L. López, Dr. C. Durio, Dr. A. Daidouh, Prof. C. Pico, Prof. Dr. M.-L. Veiga
Depto. Química Inorgánica I
Facultad de Ciencias Químicas
Universidad Complutense de Madrid
28040-Madrid (Spain)
Fax number: (+34) 913-944-352
E-mail: mlveiga@quim.ucm.es

DOI: 10.1002/chem.200305164

tals for X-ray structure determination were obtained, powdered pure phases were not prepared in most cases. This fact precludes carrying out further studies on properties and, in consequence, their applications cannot be envisaged.

From the isolation and characterisation of a good number of phases of the system $AM_4(PO_4)_3$, we noted that some of them showed remarkable electrical and magnetic properties.[15,16] We pointed out that the complex behaviour of these materials needed the knowledge of their magnetic structure in order to provide a complete interpretation for it.

The aim of present work is to report the room-temperature crystal structure refinement and the low-temperature magnetic structure of $KNi_4(PO_4)_3$, carried out by high-resolution neutron powder diffraction (NPD). From these results its magnetic behaviour is analysed on the basis of coexisting Ni-O-Ni superexchange with super–superexchange (Ni-O-O-Ni) magnetic interactions mediated by phosphate groups (NiO_n-PO_4-NiO_m). The magnetic structures of other related derivatives of manganese and cobalt are under study and will be reported in due course.

Results and Discussion

Crystal structure refinement: The refinement of the $KNi_4(PO_4)_3$ crystallographic structure was carried out from a high-resolution NPD pattern collected at room temperature with $\lambda = 1.911$ Å. The data were fitted using the pattern matching routine of the program Fullprof,[18] in the *Pnnm* space group, taking the parameters previously reported by some of us[15,16] as a starting point. The structural refinement was performed in this space group and the good agreement between the observed and calculated patterns is shown in Figure 1. The structural parameters calculated in the refinement are gathered in Table 2.

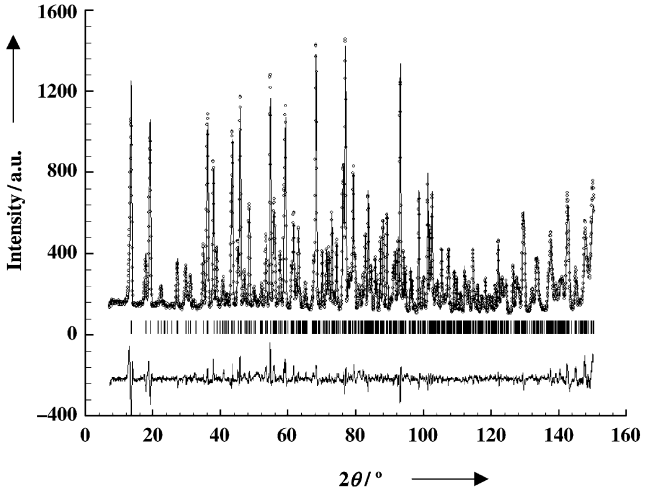

Figure 1. Observed (circle), calculated (solid line), and difference (at the bottom) neutron diffraction (D1A, ILL) profiles of $KNi_4(PO_4)_3$ at room temperature. Vertical marks correspond to the position of the allowed reflections for the crystallographic structure.

Table 2. Details of full-profile refinements from neutron diffraction pattern at room temperature for $KNi_4(PO_4)_3$.

space group	*Pnnm*
a [Å]	9.474(9)
b [Å]	16.203(8)
c [Å]	6.145(7)
V [Å^3]	943.55(7)
Z	4
reflections	577
parameters	71
$R_p = \Sigma \lvert y_{i,obsvd} - (1/c) y_{i,calcd} \rvert / \Sigma y_{i,obsvd}$	5.04
$R_{wp} = \{\Sigma w_i \lvert y_{i,obsvd} - (1/c) y_{i,calcd} \rvert^2 / \Sigma w_i [y_{i,obsvd}]^2\}^{1/2}$	6.69
$R_b = [\Sigma \lvert I_{obsd} - I_{calcd} \rvert] / \Sigma I_{obsd}$	4.31
χ^2	5.71

We also tried the space group *Amam* in which $NaNi_4(PO_4)_3$ phosphate[13] had been described from single-crystal data, but no good fitting was achieved. Therefore no change of space group is detected with respect our previous results from XRD data.

In this refinement three independent crystallographic sites for the nickel and phosphorus atoms are present in the compound. The final refined positional and thermal parameters are given in Table 3. The main interatomic distances, angles

Table 3. Final refined positional and thermal parameters from the neutron diffraction pattern (D1A) at room temperature for $KNi_4(PO_4)_3$.

Atom	Site	x	y	z	β [Å^2]
K	4g	0.7966(6)	0.033(1)	0.5	1.77(2)
Ni1	4g	0.5345(7)	0.091(9)	0	0.90(6)
Ni2	4g	0.9872(6)	0.1423(2)	0	0.79(7)
Ni3	8h	0.2486(9)	0.2040(6)	0.2508(1)	1.07(2)
P1	4g	0.5407(5)	0.1633(7)	0.5	1.36(2)
P2	4g	0.9555(8)	0.2204(4)	0.5	0.63(1)
P3	4g	0.2091(1)	0.0356(1)	0	1.19(1)
O1	4g	0.3787(7)	0.1337(7)	0.5	1.08(1)
O2	4g	0.1135(5)	0.2242(1)	0.5	1.02(1)
O3	8h	0.5887(3)	0.1169(4)	0.2996(8)	1.08(8)
O4	4g	0.3941(4)	0.1883(7)	0	1.26(1)
O5	4g	0.6105(4)	0.2509(2)	0.5	0.94(1)
O6	4g	0.8657(9)	0.0445(1)	0	1.40(1)
O7	8h	0.1587(4)	0.090(2)	0.1975(1)	0.95(8)
O8	8h	0.8928(5)	0.1817(2)	0.7070(8)	1.42(1)
O9	4g	0.3638(7)	0.0209(2)	0	1.53(1)

and bond valence sums (BVS) around cations for the potassium nickel orthophosphate are listed in Table 4. The potassium cations adopt a six-fold coordination in a distorted trigonal prism. The three kinds of Ni atoms are arranged in distorted trigonal bipyramids, labelled Ni1, and in octahedra, Ni2 and Ni3. The phosphorus atoms form tetrahedral polyhedra that are slightly distorted. As we can see in Table 4, in all cases, their bond length mean values and the BVS's are in good agreement with the sum of the ionic radii[19] and calculated valence for all atoms, respectively.

The projection of the overall structure in the *bc* plane (Figure 2) shows its complexity, which can be rationalized as being made up of $[Ni_4(PO_4)_3]$ groups connected in such a way that tunnels parallel to the *a* axis are formed in which the potassium cations are located. The Ni–O framework will be the primary focus of this description in order to rational-

Table 4. Main interatomic distances [Å], angles [°] and bond valence sums around cations for $KNi_4(PO_4)_3$.

KO_6					
K–O3	2.691(5) ×2	K–O7	2.761(6) ×2	K–O8	2.873(1) ×2
mean	2.775				
Shannon[a]	2.78				
valence sum 1.07 1					

$P1O_4$		$P(2)O_4$		$P3O_4$	
P1–O1	1.544(1)	P2–O2	1.498(9)	P3–O6	1.479(1)
P1–O3	1.512(6) ×2	P2–O4	1.588(1)	P3–O7	1.576(6) ×2
P1–O5	1.565(1)	P2–O8	1.538(4) ×2	P3–O9	1.586(1)
mean	1.533	mean	1.541	mean	1.554
Shannon[a]	1.57	Shannon[a]	1.57	Shannon[a]	1.57
valence sum	5.02(5)	valence sum	4.94(5)	valence sum	5.11(6)

$Ni1O_5$ dimers		$Ni2O_6$ isolated		$Ni3O_6$ chains	
Ni1– O3	1.954(5) ×2	Ni2– O5	2.087(5)	Ni3– O1	2.026(5)
Ni1– O4	2.051(8)	Ni2– O6	1.958(8)	Ni3– O2	2.023(5)
Ni1– O9	1.985(8)	Ni2– O7	2.197(5) ×2	Ni3– O4	2.083(5)
Ni1– O9	2.067(8)	Ni2– O8	2.109(5) ×2	Ni3– O5	2.159(5)
				Ni3– O7	2.058(5)
				Ni3– O8	2.315(5)
mean	2.002	mean	2.109	mean	2.111
Shannon[a]	2.03	Shannon[a]	2.10	Shannon[a]	2.10
valence sum	1.97(1)	valence sum	1.89(1)	valence sum	1.92(1)

$Ni1O_5$ dimers		$Ni2O_6$ isolated		$Ni3O_6$ chains	
O3-Ni1-O3	140.3(9)	O5-Ni2-O6	178.2(7)	O1-Ni3-O2	81.2(5)
O3-Ni1-O4	91.3(8)	O5-Ni2-O7	83.9(5) ×2	O1-Ni3-O4	97.8 (1)
O3-Ni1-O9	109.8(8)	O5-Ni2-O8	89.1(5) ×2	O1-Ni3-O5	174.7(3)
O3-Ni1-O9	92.9	O6-Ni2-O7	178.2(7)×2	O1-Ni3-O7	98.2(1)
O4-Ni1-O9	85.2(8)	O6-Ni2-O8	89.9(7)	O1-Ni3-O8	85.8(6)
O4-Ni1-O9	167.5(4)	O7-Ni2-O7	67.7(4)	O2-Ni3-O4	176.8(3)
O9-Ni1-O9	82.3(5)	O7-Ni2-O8	155.4(3) ×2	O2-Ni3-O5	95.8(5)
		O7-Ni2-O8	88.2(7) ×2	O2-Ni3-O7	90.1(2)
		O8-Ni2-O8	115.3(4)	O2-Ni3-O8	108.8(7)
				O4-Ni3-O5	84.8(8)
				O4-Ni3-O7	93.0(2)
				O4-Ni3-O8	68.1(7)
				O5-Ni3-O7	86.1(1)
				O5-Ni3-O8	90.9(4)
				O7-Ni3-O8	161.1(2)

[a] Shannon ionic radii, see reference [19].

ize the magnetic behaviour. This framework can be decomposed in three different fragments for clarity. The Ni3 arrangement defines one-dimensional chains of edge-shared octahedra along the *c* axis that condense with Ni2 isolated octahedra to form layers parallel to the *ac* plane (Figure 2b). These $Ni2O_6$ octahedra, which are situated between the Ni3 chains, share two edges with one chain (left) and two of the vertices with two apical oxygens on the other adjacent Ni3 chain (right) to form an extended lattice along the *a* axis. The trigonal bipyramids (or pseudo-square pyramids) $Ni1O_5$ share an equatorial edge (Figure 2c) and these units are linked to the Ni3/Ni2 layers through the third equatorial corner and an oxygen atom of the edge-shared Ni3 chains in order to extend the Ni–O framework along the *b* axis. Finally, $Ni1_2O_8$ dimers are also connected to $Ni2O_6$ isolated octahedra through PO_4 tetrahedra by sharing corners, thus forming Ni–O/PO_4 layers in the *bc* plane (Figure 2d). Note that shared corners of PO_4 tetrahedra lie in the plane and their fourth corner alternately points towards and away from the above layers and belongs to the common edge of the $(Ni3O_8)_\infty$ chains. Therefore, two parallel edge-shared $(Ni3O_8)_\infty$ chains are orientated approximately orthogonal to each other with respect to their square planes, but are not in direct contact (see Figure 2a,b).

Magnetic properties: Variable temperature magnetic susceptibility measurements of $KNi_4(PO_4)_3$ have been carried out on a powdered sample over the temperature 4.2–300 K range. Figure 3 shows the temperature dependence of the magnetic susceptibility and its reciprocal for this compound. At temperatures above 50 K the thermal evolution of χ_m follows a Curie–Weiss law, $\chi_m = C_m/(T-\theta)$, with $C_m = 1.4\ \mathrm{emu\,K\,mol^{-1}}$ Ni^{2+}, and $\theta = 0.82$ K. From the difference between the experimental (3.34 μ_B) and theoretical (2.83 μ_B) values of the magnetic moments encountered, some magnetic interactions between the paramagnetic Ni^{2+} ions are to be expected.

Below 50 K, the molar magnetic susceptibility increases noticeably with decreasing temperature and reaches a maximum at 7 K, indicating that a long magnetic order is established at this temperature. Figure 4 shows the $\chi_m T$ versus T curve, and we can observe that the $\chi_m T$ product increases when temperature decreases, showing a transition at the Néel temperature of 40 K and reaching a sharp maximum at 20 K. This behaviour can be attributed to the dominant magnetic exchange interaction of ferromagnetic (FM) in nature.[20] However, it s interesting to note a more complex behaviour, evidenced by the maxima observed in the χ_m graph, that can be attributed to a weakly antiferromagnetic (AFM) component.[21]

The presence of the above FM component is confirmed by the magnetization versus magnetic field measurements shown in Figure 5. In the isothermal magnetization curve corresponding to $T = 2$ K a remanent magnetization is observed, its value being around 2.15 μ_B per formula unit. Although some magnetization still remains at $T = 14$ K, around 1.78 μ_B per formula unit, at higher temperatures, for instance at 50 K (not shown), the field dependence of the magnetization is linear and no hysteresis is observed; this indicates a paramagnetic behaviour. The hysteresis loops do not saturate even at fields as high as 50 kOe suggesting that an AFM component is also present.

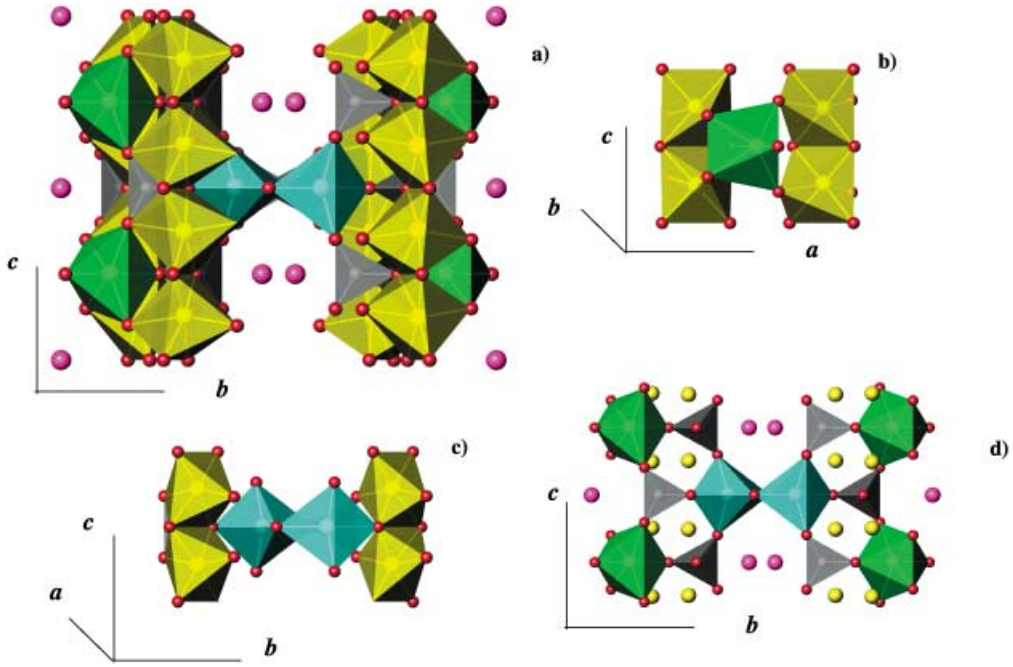

Figure 2. Crystal structure of $KNi_4(PO_4)_3$. Colour codes: Ni1 blue, Ni2 green, and Ni3 yellow polyhedra; PO_4 groups dark tetrahedra. a) Polyhedral view of the crystal structure of $KNi_4(PO_4)_3$ in the [100] direction. b) Connections between $(Ni3O_8)_\infty$ chains and $Ni2O_6$ octahedra in the [010] direction. c) Connections between $(Ni3O_8)_\infty$ chains and $(Ni1_2O_6)$ dimers. d) Connections between $(Ni1_2O_8)$ dimers and $Ni2O_6$ octahedra through PO_4 groups.

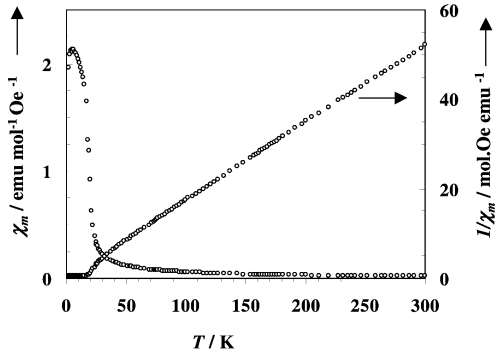

Figure 3. Temperature dependence of molar magnetic susceptibility (χ_m) and inverse ($1/\chi_m$) for $KNi_4(PO_4)_3$.

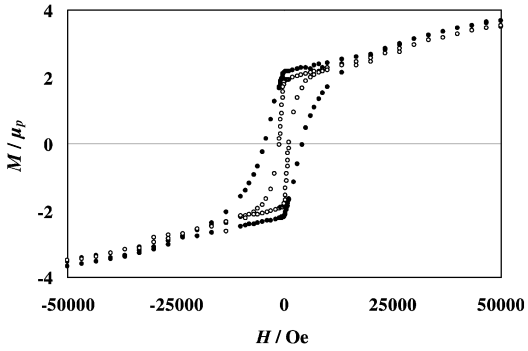

Figure 5. Magnetization versus magnetic field for $KNi_4(PO_4)_3$ at two temperatures: dark circle $T=2$ K and open circle $T=14$ K.

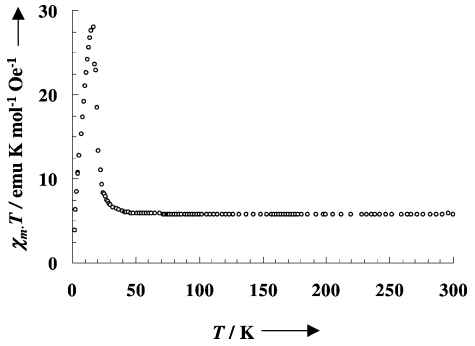

Figure 4. Temperature dependence of $\chi_m T$ for $KNi_4(PO_4)_3$.

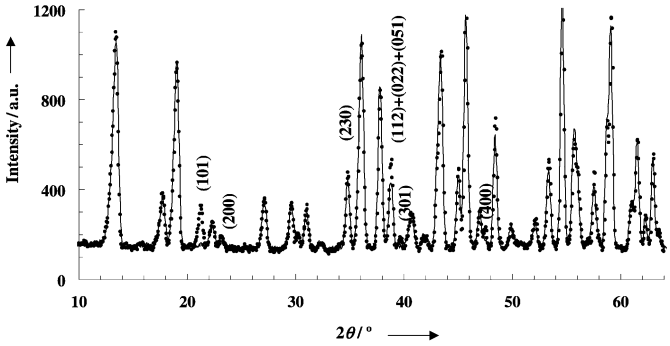

Figure 6. Observed neutron diffraction patterns of $KNi_4(PO_4)_3$ at 300 K (line) and 5 K (dots).

Magnetic structure determination: Figure 6 shows the NPD patterns collected at 300 and 5 K. By comparing both patterns noticeable changes are observed in certain Bragg reflections, which are all permitted in the space group *Pnnm*. From the pattern acquired at T = 5 K some of them, such as the (101), (200), (301) and (400) reflections, start to be ob-

served and others, such as the (230) and (112)/(022)/(051) reflections, increase in intensity. Thus the NPD pattern at room temperature is characteristic of only the nuclear scattering and the observed variations should be due to magnetic interactions, according to the above magnetic measurements.

This behaviour corresponds to the onset of a magnetic ordering in good agreement with previous studies in related systems.[22] All magnetic peaks can be indexed with a propagation vector $\boldsymbol{k}=(000)$, referring to the room-temperature unit cell, indicating that both the magnetic and nuclear cells are similar.

Group theory analysis: The possible magnetic structures compatible with the *Pnnm* crystal symmetry have been evaluated with help of Bertaut's macroscopic theory,[23] which allows one to determine the symmetry constraints between each magnetic moment of all Ni^{2+} belonging to the same general crystallographic positions. Nevertheless, the present problem is quite complex, because the magnetic cations occupy three different crystallographic sites, giving rise to three magnetic sub-lattices that seem to interact simultaneously: one of them arises from general sites 8h (named Ni3 in Table 3) and the remaining nickel cations are located in the special sites 4g (labelled as Ni1 and Ni2). By using the method developed by Bertaut and taking into account the restrains imposed by the independent symmetry elements of the space group *Pnnm* along the three directions *x*, *y* and *z*, the orientations of the magnetic moments in every sub-lattice were calculated. The basis vectors obtained for each irreducible representation Γ_i, according to the projection operator method, are reported in Table 5.

Table 5. Basis vectors for *Pnnm* and $k=0$. Atomic positions for Ni1 and Ni2: 1. $(x,y,0)$; 2. $(-x, -y, 0)$; 3. $(-x+{}^1/_2, y+{}^1/_2, {}^1/_2)$; 4. $(x+{}^1/_2, -y+{}^1/_2, {}^1/_2)$; and for Ni3: 1. (x,y,z); 2. $(-x, -y, z)$; 3. $(-x+{}^1/_2, y+{}^1/_2, -z+{}^1/_2)$; 4. $(x+{}^1/_2, -y+{}^1/_2, -z+{}^1/_2)$.[a,b]

	Ni1 and Ni2			Ni3		
	x	*y*	*z*	*x*	*y*	*z*
Γ_1	*A*	*G*	–	*A*	*G*	*C*
Γ_2	*G*	*A*	–	*G*	*A*	*F*
Γ_3	–	–	*A*	*C*	*F*	*A*
Γ_4	–	–	*G*	*F*	*C*	*G*
Γ_5	–	–	*C*			
Γ_6	–	–	*F*			
Γ_7	*C*	*F*	–			
Γ_8	*F*	*C*	–			

[a] $F=S_1+S_2+S_3+S_4$; $A=S_1-S_2-S_3+S_4$; $G=S_1-S_2+S_3-S_4$; $C=S_1+S_2-S_3-S_4$. [b] Two sets of positions related by $\bar{1}$.

The agreement between the observed and calculated diffraction patterns for each possible magnetic structure has been tested. After checking all of these solutions, it was found that the best fitting was obtained from $(C_x, F_y, 0)$ for Ni1, and $(0, F_y, 0)$ for Ni2, both located on special sites 4g, and from $(C_x, F_y, 0)$ for Ni3, which are placed on general sites 8h. The discrepancy factors and the calculated magnetic moments are shown in Table 6. For this solution, the good agreement between the observed and calculated patterns at $T=5$ K can be seen in Figure 7. The best refinement corresponds to the magnetic structure of $KNi_4(PO_4)_3$ depicted in Figure 8.

Table 6. Magnetic moment and discrepancy factors associated with the models for $T=5$ K.[a]

	C_x	F_y	A_z	μ [μ_B]
Ni1	−1.07(4)	1.42(3)	–	1.78
Ni2	0	−1.98(4)	–	1.98
Ni3	1.18(3)	−1.77(6)	0	2.12

[a] $R_m=5.40$, $R_B=4.31$.

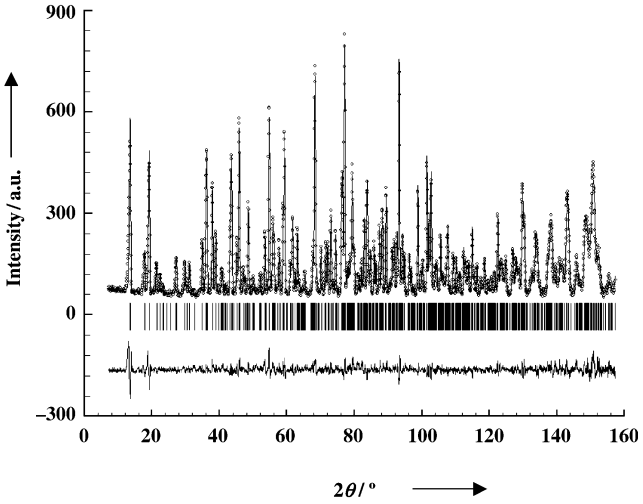

Figure 7. Observed and calculated neutron diffraction patterns of $KNi_4(PO_4)_3$ at 5 K and difference between them.

As it was above described, the crystal structure is built by arrangements of three types of entities formed by nickel polyhedra sharing corners and edges, and linked by PO_4 isolated tetrahedral units. Let us recall how such entities are arranged in the crystal structure:

1) Ni3 octahedral chains run parallel to the *c* axis.
2) Ni2 isolated octahedra are linked to the Ni3 chains, forming triangular groups (being around 60° the angles Ni(3)-Ni2-Ni3).
3) Ni1 form trigonal bipyramidal dimers that link parallel to the above-mentioned Ni3/Ni2 chains.

In the magnetic structure (see Figure 8) all these main entities interact as follows:

1) Ni3 octahedral chains show a FM component along the *y* direction and, with respect to the *x* component, the magnetic structure consists of FM chains that are antiferromagnetically coupled (Figure 8b).
2) Ni2 isolated octahedra possess a unique FM component along the *y* direction. Between Ni3 and Ni2 a non-collinear arrangement is found, consistent with the edge-shared triangular Ni^{2+} arrangement, which is marked in Figure 8a for clarity.

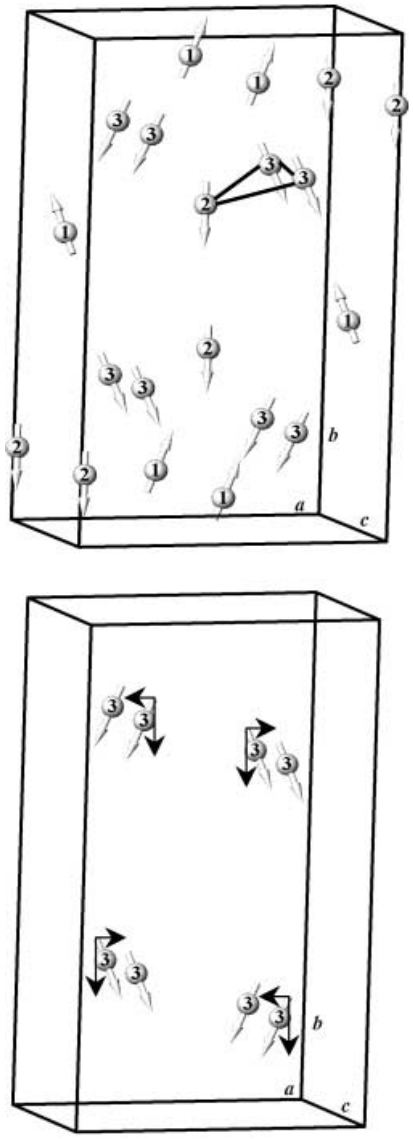

Figure 8. Magnetic structure model of $KNi_4(PO_4)_3$ showing the three Ni sub-lattices and their respective moments.

3) Ni1 trigonal bipyramidal dimers are ferromagnetically ordered in the *ab* plane.
4) Finally, both entities, Ni3 and the next neighbours Ni1, are antiferromagnetically coupled.

Although the overall refined model is FM, the arrangement of the moments allows the existence of a weak AFM component in both *x* (between Ni3 atoms) and *y* directions (i.e., between Ni1 and Ni3 neighbouring atoms).

Conclusions

In the magnetization versus magnetic field measurements (see Figure 5) a remanent magnetization is observed at $T=2$ and 14 K; this is in good agreement with the above magnetic structure model determined from NPD data. In the low-temperature structure a strong magnetic component develops along the *b* direction. However, a maximum is observed at around 7 K that can be attributed to an AFM coupling between Ni3 and Ni1.

The ordered magnetic moments obtained at 5 K, 1.78 μ_B for Ni1, 1.98 μ_B for Ni2, and 2.12 μ_B for Ni3, agree well with those expected for Ni atoms in the divalent oxidation state, Ni^{2+}, with $S=1$ (ordered moment 2 μ_B). The refined magnetic moments of the Ni^{2+} ions in an octahedral environment are always higher than those with a bipyramidal trigonal geometry. The slight observed differences can be attributed to the distinct crystal effects.[24]

The magnetic structure of $KNi_4(PO_4)_3$ shown in Figure 8 consists of AFM arrangements between the $(Ni3O_8)_\infty$ octahedral chains and $(Ni1_2O_8)$ dimers, in trigonal bipyramidal coordination, with their magnetic moments orientated on the *ab* plane. On the other hand, the fact that the Ni2 sublattice becomes ordered according to the basis functions of the same irreducible representation, as occurs in the Ni3 sub-lattice, implies that the Ni2 sub-lattice ordering is probably provoked by the local magnetic field created by the ordered Ni3 moments on the Ni2 sites. Recall that the Ni2 atoms are located between two chains of $(Ni3O_8)_\infty$ sharing edges or corners. With respect to the *x* component, it is interesting to note that both $(Ni3O_8)_\infty$ chains are antiferromagnetically coupled, giving way to a zero magnetic field at the Ni2 site. Therefore, the ferromagnetic *y* component of the Ni3 atoms gives rise to a non-zero magnetic field at the Ni2 sites and is the responsible for the Ni2 sub-lattice ordering. Something similar has been described for $NdMnO_3$.[25]

Spontaneous static ordering of the magnetic moments at low temperatures is caused by exchange interactions between the moments, making it energetically favourable for them to align either parallel or anti-parallel. Superexchange interactions are well understood for a simple cation–anion–cation pathway with interactions strongly AFM for a linear 180° Ni-O-Ni bond angle and FM for an angle of 90°. The higher value observed up to now for FM interactions in Ni^{II} compounds is 104°.[26]

The magnetic structure of $KNi_4(PO_4)_3$ allows us to establish several exchange pathways[20,27,28] (see Figure 9):

1) Superexchange intradimer interactions through oxygen atoms involving metal $d_{x^2-y^2}$ orbitals from edge-sharing nickel polyhedra, both in $(Ni1_2O_8)$ trigonal bipyramidal

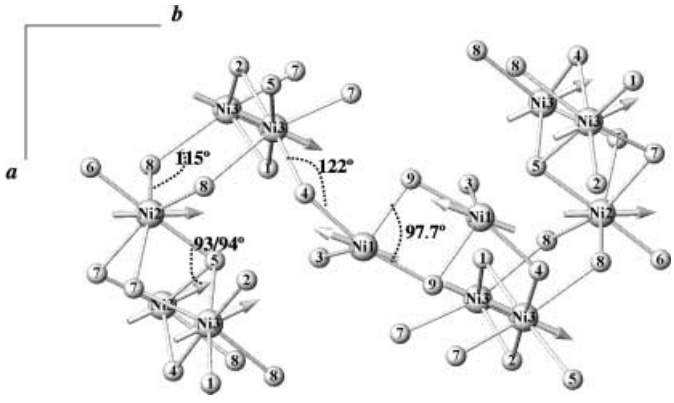

Figure 9. Exchange pathways for $KNi_4(PO_4)_3$.

dimers and in $(Ni3O_8)_\infty$ octahedral chains. Shorter Ni3-O4-Ni3 bond lengths (2×2.08 Å and angle 95.5°) offer a stronger FM exchange pathway than Ni3-O5-Ni3 bonds (2×2.15 Å and 92.2°); hence, this gives rise to a more efficient orbital overlap. In the same way, in the $(Ni1_2O_8)$ units, in which the angles are only somewhat higher (97.7°) intradimer FM couplings are also favourable.

2) AFM superexchange interactions between $(Ni1_2O_8)$ dimers and their neighbour chains, through the O4 atoms or PO_4 groups, are favoured by the higher bond angle Ni3-O4-Ni1 (122°) and the relatively short bond lengths (2.05 Å; Figure 9). Connections between the Ni3 chains and Ni1 dimers, as well as between Ni2 isolated octahedra and Ni1 dimers, are also available through the bonding phosphate groups (i.e., Ni1-O-P-O-Ni3 or Ni1-O-P-O-Ni2, respectively). In this sense, weak M-O-P-O-M superexchange between octahedra occurs in $KBaFe_2(PO_4)_3$[29] between 4.2 and 3.9 K, and stronger interactions are observed in $Na_3Fe_2(PO_4)_3$,[30] $NaFeP_2O_7$[31]and $Fe_3(PO_4)_2$,[32] with Néel temperatures of 29, 47 and 44 K, respectively. As the magnetic ordering temperature of $KNi_4(PO_4)_3$ is closer (40 K) it would seem more likely that the superexchange pathways through the PO_4 group will not be negligible.
3) Superexchange interactions between $(Ni3O_8)_\infty$ chains and $(Ni2O_6)$ isolated octahedra may operate through the O7 and O8 atoms, with the former providing the greatest opportunity for orbital overlap Ni3-O7-Ni2 (bond lengths 2.19, 2.05 Å and angle 90°). Therefore, FM interactions between them must be operative.
4) The presence of dimers $(Ni1_2O_8)$ seems to be responsible for the interchains FM coupling of $(Ni3O_8)_\infty$ and, in consequence, for the overall ferromagnetism of the structure.

The magnetic structures of other related derivatives of manganese ($KMn_4(PO_4)_3$) and cobalt ($KCo_4(PO_4)_3$) show remarkable differences with this phase of nickel and also between themsleves; the results will be reported in due course.

Experimental Section

Polycrystalline samples of $KNi_4(PO_4)_3$ were prepared by the "liquid mix" technique[33] from powdered mixtures of KNO_3, $Ni(NO_3)_2{\cdot}6H_2O$, and $(NH_2)_2HPO_4$ (all reactants were supplied by Merck, Germany), in stoichiometric ratios. The samples were obtained by firing in alumina crucible at temperatures above 1173 K for 24 h.

Neutron powder diffraction data were performed at different temperatures on the D1A high-resolution powder diffractometer ($\lambda = 1.9110$ Å) at the Institute Laue–Langevin (Grenoble, France). Diffraction patterns were analysed by the Rietveld[34] method and the Fullprof program.[18]

The magnetic susceptibility measurements were performed in a commercial superconducting quantum interference device magnetometer, Quantum Design Magnetic Properties Measurement System 5S, on powder samples in a temperature range from 1.8 K to 300 K under an applied magnetic field of 5000 Oe. The magnetic field isothermal variations up to 50 kOe were obtained with the aid of a Quantum Design Physical Properties Magnetic System, which allowed for the experimental setting of highly homogeneous magnetic field at specific temperatures.

Acknowledgement

Financial support through research Projects MAT2000–1585 and MAT2002–01288 (CICYT, Spain) are acknowledged. We also thank Dr. Gabriel Cuello for assistance with the D1A diffractometer and the ILL facilities.

[1] A. E. C. Green, C. R. Wiebe, J. E. Greedan, *Solid State Sci.* **2002**, *4*, 305–310.
[2] L. Chi, A. E. C. Green, R. Hammond, C. R. Wiebe, J. E. Greedan, *Solid State Sci.* **2003**, 170, 165–175.
[3] M. A. Subramanian, A. P. Ramirez, G. H. Kwei, *Solid State Ionics* **1998**, *108*, 185–191.
[4] A. I. Ruiz, J. Campo, M. L. López, J. L. Martinez Peña, C. Pico, M. L. Veiga, *Eur. J. Inorg. Chem.* **2002**, 1071–1075.
[5] M. Tackeray, *Nature Materials*, **2002**, 1, 81–82.
[6] A. K. Ivanov-Shitz, A. V. Nistuk, N. G. Chaban, *Solid State Ionics* **2001**, *139*, 153–157.
[7] G. Rousse, J. Rodríguez-Carvajal, C. Wurm, C. Masquelier, *Solid State Sci.* **2002**, *4*, 973–978.
[8] N. El Khayati, J. Rodríguez-Carvajal, F. Bourée, T. Roisnel, R. Cherkaoui, A. Boutfessi, A. Boukhari, *Solid State Sci.* **2002**, *4*, 1273–1283.
[9] J. M. Rojo, J. L. Mesa, L. Lezama, J. L. Pizarro, M. I. Arriortua, J. Rodríguez Fernández, G. E. Barberis, T. Rojo, *Phys. Rev. B* **2002**, *66*, 094406(13 pages).
[10] L. K. Elbouaanani, B. Malaman, R. Gérardin, M. Ijjaali, *J. Solid State Chem.* **2002**, *163*, 412–420.
[11] E. N. Matvienko, O. V. Yakubovich, M. A. Simonov, N. V. Belov, *Sov. Phys. Dokl.* **1981**, *26*, 633–635.
[12] M. Ben Amara, M. Vlasse, R. Olazcuaga, G. Le Flem, P. Hagenmuller, *Acta Crystallogr. Sect. C* **1983**, *39*, 936–939.
[13] J. B. Anderson, J. Moring, E. Kostiner, *J. Solid State Chem.* **1985**, *60*, 358–365.
[14] O. V. Yakubovich, O. A. Evdokimova, O. K. Mel'nikov, M. A. Simonov, *Sov. Phys. Crystallogr.* **1986**, *31*, 151–154.
[15] A. Daidouh, J. L. Martinez, C. Pico, M. L. Veiga, *J. Solid State Chem.* **1999**, *144*, 169–174.
[16] A. Daidouh, C. Pico, M. L. Veiga, *Solid State Ionics* **1999**, *124*, 109–117.
[17] S. Neeraj, M. L. Noy, A. K. Cheetham, *Solid State Sci.***2002**, *4*, 397–404.
[18] J. Rodríguez Carvajal; FULLPROF. XV Congress of International Union of Crystallography, Toulouse **1990**, p. 127, **1994** (Revised version).
[19] R. D. Shannon, *Acta Crystallogr. Sect. A* **1976**, *32*, 751–753.
[20] J. B. Goodenough, *Magnetism and Chemical Bond*, Krieger, New York, **1976**.
[21] W. M. Reif, J. H. Zhang, C. C. Torardi, *J. Solid State Chem.* **1986**, *62*, 231–234.
[22] S. T. Bramwell, A. M. Buckley, P. Day, *J. solid State Chem.* **1994**, *111*, 225–228.
[23] E. F. Bertaut, *Acta Crystallogr. Sect. A* **1968**, *24*, 217–231.
[24] M. E. Foglio, M. C. dos Santos, G. E. Barberis, J. M. Rojo, J. L. Mesa, L. Lezama, T. Rojo, *J. Phys. Condens. Matter* **2002**, *14*, 2025–2030.
[25] A. Moñoz, J. A. Alonso, M. J. Martinez-Lope, J. L. Garcia-Muñoz, M. T. Fernández-Diaz, *J. Phys. Condens. Matter* **2000**, *12*, 1361–1376.
[26] N. El Khayati, R. Cherkaoui El Moursli, J. Rodríguez-Carvajal, G. André, N. Blanchard, F. Bourée, G. Collin, T. Roisnel, *Eur. Phys. J.* **2001**, *B22*, 429–442.
[27] O. Khan, *Inorg. Chem.* **1984**, *23*, 105–108.
[28] O. Khan, *Struct. Bonding* **1987**, *68*, 89–91.
[29] P. D. Battle, P. D. Cheetham, A. K. Harrison, W. T. A. Long, G. L. Long, *J. Solid State Chem.* **1986**, *62*, 16–18.
[30] G. Rousse, J. Rodríguez-Carvajal, C. Wurm, C. Masquelier, *Chem. Mater.* **2001**, *13*, 4527–4536.

[31] R. C. Mercader, A. Terminiello, G. J. Long, D. G. Reichel, K. Dickhaus, R. Zysler, R. D. Sanchez, M. Tovar, *Phys Rev. B* **1990**, *42*, 25 – 30
[32] J. K. Warner, A. K. Cheetham, A. G. Nord, R. B. Von Dreele, M. Yethiraj, *J. Mater. Chem.* **1992**, *2*, 191 – 196.
[33] M. Pechini, *US. Patent*, **1996**, 3 231/328.
[34] H. M. Rietveld, *J. Appl. Crystallogr.* **1969**, *2*, 65 – 71.

Received: May 20, 2003
Revised: September 10, 2003 [F5164]

